

Active Inference in Hebbian Learning Networks

Ali Safa^{1,2,3}, Tim Verbelen⁴, Lars Keuninckx², Ilja Ocket², André Bourdoux²,
 Francky Catthoor^{1,2}, Georges Gielen^{1,2}, and Gert Cauwenberghs³

¹ imec, Leuven, Belgium

² ESAT, KU Leuven, Belgium

³ University of California at San Diego, La Jolla, USA

⁴ VERSES Research Lab, Los Angeles, California, USA

Ali.Safa@imec.be

Abstract. This work studies how brain-inspired neural ensembles equipped with local Hebbian plasticity can perform active inference (AIF) in order to control dynamical agents. A generative model capturing the environment dynamics is learned by a network composed of two distinct Hebbian ensembles: a *posterior* network, which infers latent states given the observations, and a *state transition* network, which predicts the next expected latent state given current state-action pairs. Experimental studies are conducted using the Mountain Car environment from the OpenAI gym suite, to study the effect of the various Hebbian network parameters on the task performance. It is shown that the proposed Hebbian AIF approach outperforms the use of Q-learning, while *not requiring* any replay buffer, as in typical reinforcement learning systems. These results motivate further investigations of Hebbian learning for the design of AIF networks that can learn environment dynamics without the need for revisiting past buffered experiences.

Keywords: Active Inference · Hebbian Learning · Sparse Coding.

1 Introduction

The study of Sparse Coding [1], [2], [3], [4] and Predictive Coding [5], [6], [7] networks has gained much attention for understanding the mechanisms underlying learning and inference in the brain [8]. In particular, it has been shown that the learning of the *weight dictionary* used to project the input signals into sparse codes can be conducted via the biologically-plausible Hebbian learning mechanism [9], with experimental evidence behind this mechanism observed in the brain [10], [11]. Hebbian learning differs from the widely-used *back-propagation of error* (backprop) technique due to its *local* nature [7], [12], [13], where the weight w_j of neuron i is modified via a combination f of the weight's input x_j and the neuron's output y_i (with η_d the learning rate parameter):

$$w_j \leftarrow w_j + \eta_d f(y_i, x_j) \quad (1)$$

When applied to layers that embark some form of competition between their neurons, the Hebbian mechanism in (1) leads to the *unsupervised* learning of complementary features from the input signals [14].

At the same time, Active Inference (AIF) has gained huge interest as a *first-principle* theory, explaining how biological agents evolve and perform actions in their environment [15], [16]. In recent years, the use of deep neural

networks (DNNs) for parameterizing generative models has gained much attention in AIF research [17], [18], [19]. Deep AIF systems are typically composed of a *posterior* network $q_{\Phi_P}(s_l|o_{l-1}, a_{l-1})$, inferring the latent state s_l given an incoming observation-action pair $\{o_{l-1}, a_{l-1}\}$, and a *state-transition* network $p_{\Phi_S}(s_l|s_{l-1}, a_{l-1})$, predicting the next latent state s_l given the current state-action pair $\{s_{l-1}, a_{l-1}\}$ [17]. The state-transition network is used to generate the agent’s roll-outs for different policies in order to compute the Expected Free Energy associated to each policy [17]. Finally, a *likelihood* network $p_{\Phi_L}(o_l|s_l)$ reconstructing the input observation o_l from the latent state s_l can also be implemented [20]. Each network parameterizes its respective density function through weight tensors Φ_P, Φ_S and Φ_L .

In this work, we aim to study how AIF can be performed in Hebbian learning networks *without resorting to backprop* (as typically used in deep AIF systems). Experiments conducted in the OpenAI Mountain Car environment [21] show that the proposed Hebbian AIF approach outperforms the use of Q-learning and compares favorably to the backprop-trained Deep AIF system of [17], while *not requiring* any replay buffer, as in typical reinforcement learning systems [22]. Our derivations and experiments add to a growing number of work addressing the study of Hebbian Active Inference [23], [24].

This paper is organized as follows. Background theory about Hebbian learning networks is provided in Section 2. Our Hebbian AIF methods are covered in Section 3. Experimental results are shown in Section 4. Conclusions are provided in Section 5.

2 Background Theory on Hebbian Learning Networks

Inspired by previous works that model the neural activity of biological agents through Sparse Coding [5], [9] (such as in the *mushroom body* of an insect’s brain [25]), we model each individual Hebbian Ensemble layer of our networks as an identically-distributed Gaussian likelihood model with a Laplacian prior on the neural activity c :

$$p(c|o, \Phi) \sim \exp(-\|\Phi c - o\|_2^2) \exp(-\lambda\|c\|_1) \quad (2)$$

where o is the input of dimension N , c is the output of dimension M , Φ is the $N \times M$ weight matrix of the layer (also called *dictionary*), and λ is a hyper-parameter setting the scale of the Laplacian prior. Choosing a Laplacian prior is motivated by the fact that it promotes sparsity in the output neural code in a way similar to how sparsity is induced in networks of Spiking Leaky Integrate-and-Fire neurons, modelling cortical neural activity [9].

Under Sparse Coding (2), inference of c and learning of Φ is carried via [9]:

$$C, \Phi = \arg \min_{C, \Phi} \sum_l \|\Phi c_l - o_l\|_2^2 + \lambda\|c_l\|_1 \quad \mathbf{with} \quad C = \{c_l, \forall l\} \quad (3)$$

which can be solved via Proximal Stochastic Gradient Descent [26], by *alternating* between: *a)* the inference of c_l , given the current input o_l and the weight Φ and *b)* the learning of Φ , given the current c_l and o_l .

Hence, we instantiate Hebbian layers as the dynamical system given in (4), where T denotes the transpose, η_c is the coding rate, η_d is the learning rate and $\mathbf{Prox}_{\lambda\|\cdot\|_1}$ is the proximal operator to the l_1 norm (non-linearity) [27]. For each input o_i , the neural and weight dynamics of the Hebbian network follows the

update rules in (4) for an arbitrary number of iterations (set to 100 in this work as a good balance between speed of convergence and convergence quality), in order to infer the corresponding c_l and learn Φ [9].

$$\begin{cases} c_l \leftarrow \mathbf{Prox}_{\lambda|\cdot|_1} \{c_l - \eta_c \Phi^T (\Phi c_l - o_l)\} \\ \Phi \leftarrow \Phi - \eta_d (\Phi c_l - o_l) c_l^T \end{cases} \quad (4)$$

with $\mathbf{Prox}_{\lambda|\cdot|_1}$ acting as the neural non-linearity:

$$\mathbf{Prox}_{\lambda|\cdot|_1}(c_i) = \text{sign}(c_i) \max(0, |c_i| - \eta_c \lambda), \forall i \quad (5)$$

From a neural point of view, the dynamical system of (4) can be implemented as the network architecture in Fig. 1, where all weight updates follow the standard Hebbian rule (1) [9].

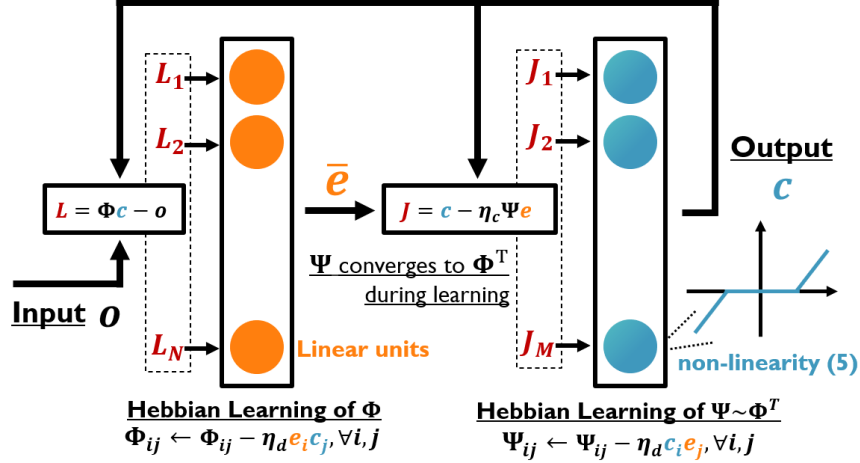


Fig. 1. Baseline Hebbian network architecture used in this work. The dynamics of the network follow (4) and minimize (3), given subsequent input vectors o . Each layer possesses its own weight matrix Φ, Ψ which evolve through Hebbian plasticity ($\Psi \sim \Phi^T$ in (4)), as an independent, local set of weights.

3 Active Inference in Hebbian Learning Networks

In this Section, we show how the Hebbian network described above in Section 2 is utilized in order to build an AIF system. First, we describe how Variational Free Energy minimization can be performed by a cascade of two Hebbian networks: a *state-transition* network predicting the next latent states given the previous ones, and a *posterior* network providing latent states given input observations. Crucially, it is shown that Free Energy minimization necessitates top-down Hebbian learning connections from the *state-transition* network towards the *posterior* network, steering the posterior output activity towards the state-transition output during learning. Then, we show how the Expected Free Energy is computed by generating state transition roll-outs.

3.1 Minimizing the Variational Free Energy

The Variational Free Energy can be decomposed as [17] [28] (where \mathbb{E} denotes the expected value):

$$\mathcal{F} = D_{KL}[q_{\Phi_P}(s_l|o_{l-1}, a_{l-1})||p_{\Phi_S}(s_l|s_{l-1}, a_{l-1})] - \mathbb{E}_q[\log(p_{\Phi_L}(o_l|s_l))] \quad (6)$$

with the parametrized densities $q_{\Phi_P}, p_{\Phi_S}, p_{\Phi_L}$ described in Section 1. Since the Hebbian network architecture used in this work intrinsically provides a mean to reconstruct its input x_l in (3) (i.e., *likelihood* modelling) from its produced latent code c_l in (3) (i.e., *posterior* modelling), using the *same dictionary* parameter matrix Φ in (3) that was used to generate c_l via (4), we have $\tilde{\Phi}_L = \Phi_P$ in (6) and we will solely use Φ_P below to denote the *posterior* weight matrix.

Under the assumption of Gaussian likelihood with identity covariance in (2), the KL divergence D_{KL} in \mathcal{F} can be simplified to [29]:

$$\mathcal{F} \sim \|\Phi_S c_{S,l} - \{s_l(\Phi_P), a_l\}\|_2^2 + \|\Phi_P s_l - \{o_l, a_l\}\|_2^2 \quad (7)$$

where $s_l(\Phi_P)$ explicits the dependency of s_l on Φ_P (s_l being the posterior network output activity) and c_S denotes the output activity of the state-transition network given s_l . The Free Energy in (7) must be minimized with regard to the state transition weights Φ_S and the posterior weights Φ_P during learning:

$$\Phi_S, \Phi_P = \arg \min_{\Phi_S, \Phi_P} \|\Phi_S c_{S,l} - \{s_l(\Phi_P), a_l\}\|_2^2 + \|\Phi_P s_l - \{o_l, a_l\}\|_2^2, \forall l \quad (8)$$

This indicates that it is not only the state transition model that must be steered towards the posterior model, but also, the posterior model must be steered towards the output of the state-transition network. This effect can be achieved by re-formulating the optimization in (8) as:

$$\begin{cases} \Phi_S = \arg \min_{\Phi_S} \|\Phi_S c_{S,l} - \{s_l, a_l\}\|_2^2, \forall l & \text{(a)} \\ \Phi_P = \arg \min_{\Phi_P} \|\Phi_P s_l - \{o_l, a_l\}\|_2^2 + \|\Phi_P(\Phi_S c_{S,l}) - \{o_l, a_l\}\|_2^2 & \text{(b)} \end{cases} \quad (9)$$

Intuitively, the right-hand term in (9 b) steers the *posterior* model towards the *state-transition* model by first re-projecting the output activity of the state-transition network c_S into the latent space as $\Phi_S c_S$ (considering Φ_S fixed). Then, minimizing $\|\Phi_P(\Phi_S c_{S,l}) - \{o_l, a_l\}\|_2^2$ modifies Φ_P in order to steer its posterior output s_l towards the re-projected state-transition activity $\Phi_S c_S$ (considering $\{o_l, a_l\}$ fixed).

State-Transition Model Inspired by prior work on dictionary-based sequence modeling [30], we implement the transition model $p_{\Phi_S}(s_l|\tilde{s}_{l-1}, \tilde{a}_{l-1})$ as an *auto-regressive* Hebbian network (see Fig. 2 a), taking as input a sequence of state-and-action *history* $\tilde{s}_{l-1} = [s_{l-1}, \dots, s_{l-L_{buf}}]$, $\tilde{a}_{l-1} = [a_{l-1}, \dots, a_{l-L_{buf}}]$ and inferring the next state $\tilde{s}_l = [s_l, \dots, s_{l-L_{buf}}]$ as the re-projection of its internal sparse code c_S in the input space through the network weights Φ_S :

$$\tilde{s}_l = \Phi_S c_{S,l} \quad (10)$$

where $\Phi_{S,j}$ and $c_{S,j}$ respectively denote the weight vector and the sparse code of each layer j in the state transition network. Therefore, the state-transition network effectively projects the L_{buf} previous states (noted \tilde{s}_{l-1}) into a common

internal sparse code c_S and reconstructs the next states \tilde{s}_l by re-projection of c_S into the input space.

The state-transition network learns its weights Φ_S following (9 a) and infers its output activity c_S via sparse coding (see Section 2):

$$\Phi_{S, c_S, l} = \arg \min_{\Phi_S, c_S, l} \|\Phi_S c_S, l - \tilde{s}_l\|_2^2 + \lambda_P \|c_S, l\|_1, \forall l \quad (11)$$

where λ_P is a parameter that sets the strength of the *sparsity* of the *state-transition* output activity. (11) can therefore be implemented via the Sparse Coding-based Hebbian learning ensemble described in Section 2. This autoregressive strategy enables the network to learn state predictions using Hebbian learning, *without* the need for non-bio-plausible back-propagation through time (BPTT) [30], [31].

In order to prevent the vanishing or exploding of the state transition model when producing roll-outs further in time, we regularize the norm of the reconstructed states s_l to an arbitrary magnitude α using (12). We keep $\alpha = 5$ in our experiments in Section 4, giving a good balance for the dynamic range of the network output activity (adjusted empirically).

$$s_l = \alpha \frac{s_l}{\|s_l\|_2} \quad (12)$$

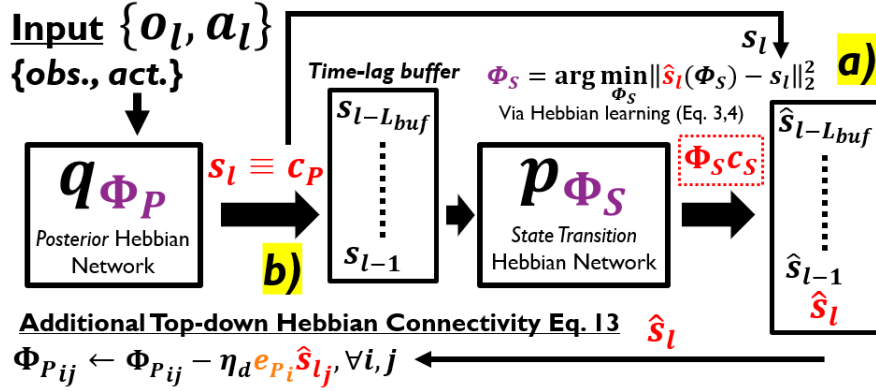


Fig. 2. Hebbian Active Inference Architecture. a) The state-transition network takes as input the L_{buf} previous latent states produced by the posterior network, and projects them onto its internal representation c_S via the learned Φ_S . When producing roll-outs, the state-transition network estimates the next state \hat{s}_l by re-projecting the output activity c_S due to $[s_{l-L_{buf}}, \dots, s_{l-1}]$ back onto the input space via (10). b) The posterior network takes observation-action pairs as input and produces latent states s (corresponding to the output in Fig. 1). In addition to the Hebbian mechanisms depicted in Fig. 1, the weights Φ_P of the posterior network are also subject to a top-down Hebbian learning mechanism for minimizing the second term in (9 b).

Posterior Model Similar to the state-transition model, we use a Hebbian ensemble as posterior model, where the internal sparse code c_P (see Fig. 2 b) is identified as the hidden state $s_l \equiv c_{P,l}$ inferred by the posterior network $q_\nu(s_l|o_{l-1}, a_{l-1})$, given the observation and action pair $\{o_{l-1}, a_{l-1}\}$ in (2).

Therefore, the posterior network learns its weights Φ_P following (9 b) and infers its output activity $s_l = c_{P,l}$ via sparse coding (see Section 2):

$$\Phi_P, c_{P,l} = \arg \min_{\Phi_P, c_{P,l}} \underbrace{\|\Phi_P c_{P,l} - \{o_l, a_l\}\|_2^2 + \lambda_Q \|c_{P,l}\|_1}_{\text{Standard Sparse Coding}} + \overbrace{\|\Phi_P(\Phi_S c_{S,l}) - \{o_l, a_l\}\|_2^2}^{\text{Top-down Connection}} \quad (13)$$

for all l , where λ_Q sets the strength of the *sparsity* of the *posterior* output activity. The left-hand *standard sparse coding* term in (13) can be implemented via the Hebbian learning ensemble described in Section 2, while the right-hand term in (13) can be implemented using *top-down* connections from the state-transition output activity c_S towards the posterior network, via the state-transition weight matrix Φ_S (see Fig. 2 b).

Finally, here again, we apply the homeostasis rule (12) to the inferred posterior state, effectively constraining s_l to lie on the α -sphere manifold.

3.2 Minimizing the Expected Free Energy

Given a policy π , the Expected Free Energy $G(\pi)$ (EFE) can be written as [32]:

$$\begin{aligned} G(\pi) &= \sum_l \mathbb{E}_{q(o_l, s_l|\pi)} [\log q(s_l|\pi) - \log p(s_l, o_l|\pi)] \\ &= \sum_l -H\{q(s_l|\pi)\} - \mathbb{E}_{q(o_l, s_l|\pi)} [\log p(s_l, o_l|\pi)] \end{aligned} \quad (14)$$

where H denotes the Shannon entropy. It can be seen in (14) that selecting a policy that minimizes the EFE entails the maximization of the posterior entropy (promoting exploration) and the joint posterior over the states and observations (reaching the desired goal) [32].

In order to reach the desired goal, we produce roll-outs of states s_l given a certain policy and approximate the term $-\mathbb{E}_q[\log p(s_l, o_l|\pi)]$ to be minimized as:

$$-\mathbb{E}_{q(o_l, s_l|\pi)} [\log p(s_l, o_l|\pi)] \sim \|s_l - s^*\|_2^2 \quad (15)$$

where s^* is the desired state that the agent must reach, corresponding to a desired observation (e.g., the agent's position). Since the observation o_l can encompass more than just the goal to be reached (i.e., the observation o_l could be both the position and the velocity of an agent, even though the desired goal is to reach a specific position regardless of the velocity), we compute the desired *goal* state s^* as:

$$s^* = \arg \max_s \int_{\omega \in D_\omega} q(s|\Omega^*, \omega) d\omega \quad (16)$$

where Ω^* contains all observations that must be reached in order to attain the desired goal and ω designates all observation modalities that are *not* taking part in defining the goal that must be reached, with D_ω their domain of definition.

In practice, (16) is estimated by averaging the output of the posterior network, while sweeping ω for a grid of possible values and keeping Ω^* fixed.

Regarding the exploration term in (14), our Hebbian network does not directly allow the estimation of the entropy $H\{q(o_l, s_l|\pi)\}$, since the network does not infer standard deviations as in a variational auto-encoder (VAE) [17]. We propose to replace the maximization of the entropy $H\{q(o_l, s_l|\pi)\}$ with a surrogate term, crafted to promote exploration as well. As a surrogate for $H\{q(o_l, s_l|\pi)\}$, we choose to maximize the variance (noted Var) of the state trajectory $s_l, \forall l = 1, \dots, L$ along time during the roll-outs. Intuitively, a state trajectory that presents lots of variation in time will promote the exploration of new states, providing a similar qualitative effect as maximizing $H\{q(o_l, s_l|\pi)\}$. Therefore, we select the policy π such that the distance to the desired state is minimized, while achieving a state trajectory variance larger than a certain threshold t_v .

$$\pi^* = \arg \min_{\pi} \mathcal{G}(\pi) = \sum_{l=1}^L \|s_l - s^*\|_2^2 \quad \text{s.t.} \quad \text{Var}(\|s_l - s^*\|_2^2, l = 1, \dots, L) \geq t_v \quad (17)$$

Given a set of N_p policies to try, t_v can be determined in an adaptive way as:

$$t_v = \beta \times \frac{1}{2} [\mathbf{max}_{\pi} (\text{Var}(\|s_l(\pi) - s^*\|_2^2, \forall l)) + \mathbf{min}_{\pi} (\text{Var}(\|s_l(\pi) - s^*\|_2^2, \forall l))] \quad (18)$$

where β is the strength hyper-parameter (empirically set to 0.5 in our experiments reported below).

4 Experimental Results

The aim of our experimental studies is to determine *i*) how the main network hyper-parameters (number of neurons, sparsity in output activity,...) impact the success rate of the proposed Hebbian AIF system; *ii*) to what extent Hebbian AIF is robust when learning without using a replay buffer and *iii*) how Hebbian AIF compares to Q-learning (which uses *dense rewards* versus *unsupervised learning* in Hebbian AIF).

4.1 Mountain Car Environment

We perform experiments in the *Mountain Car* environment from the OpenAI gym suite [21]. In this task, a car starts at a *random* position at the bottom of a hill and is expected to reach the top of a mountain within 200 time steps. The agent is subject to gravity and cannot reach the goal trivially, just by accelerating towards it. Rather, the agent must learn to gain momentum before accelerating towards the goal.

In this environment, the x-axis position x and the velocity v_x of the car constitute the input observations to the Hebbian AIF network. Before feeding the observation tuple (x, v_x) to our Hebbian network, we normalize (x, v_x) using (19) in order to equalize the dynamic range of the position and velocity signals:

$$\begin{cases} x \leftarrow \frac{x - \mu_x}{\sigma_x} \\ v_x \leftarrow \frac{x - \mu_{v_x}}{\sigma_{v_x}} \end{cases} \quad (19)$$

where (μ_x, σ_x) and $(\mu_{v_x}, \sigma_{v_x})$ denote the mean and standard deviation of the position and velocity signals respectively (estimated during random environment runs).

We use an action space constituted by two discrete actions: *accelerate to the left* and *accelerate to the right*. In addition, each action is repeated for 10 consecutive time steps once selected during the Expected Free Energy minimization in (17).

In order to compute the Expected Free Energy, we generate roll-outs of $L = 200$ time step predictions for 100 different random policies $\pi^j, j = 1, \dots, 100$ with equal probability of selecting the *accelerate to the left* or the *accelerate to the right* actions.

As learning rate for the Hebbian learning mechanism (4), we use $\eta_d = 10^{-4}$ with a *decay rate* of 0.8 applied at the end of each *successful* episode, i.e. if the episode terminates successfully, $\eta_d \leftarrow \eta_d \times 0.8$ (else no decay is applied on η_d). All weights are initialized randomly from a normal distribution with standard deviation 0.01.

In the remainder of this Sections, we perform all our experiments using a 10-fold validation approach, by reporting the success rate curves as averages over 10 different runs (with 35 episodes per runs), with different random network initializations. For each run, we compute the success rate curve using a moving average window of size 5, and report the mean success rate curve by averaging over the 10 runs, alongside with its standard deviation (see e.g. Fig. 3). We will now study the impact of the various network hyper-parameters on the achieved success rates.

4.2 Impact of the Number of Neurons in the Posterior and State Transition Networks

Fig. 3 and 4 show the effect of sweeping the number of coding neurons M_Q and M_P in both the *posterior* and *state-transition* networks. Fig. 3 shows that for $M_Q < 8$, the success rate is sub-optimal, but reaches a steady plateau around $M_Q = 8$ (orange curve in Fig. 3). Then, as M_Q is increased for $M_Q > 8$, the success rate becomes sub-optimal again, with dips in the performance along the episodes (e.g., red curve in Fig. 3). This phenomenon can be explained as follows: for $M_Q < 8$, the posterior network does not have enough parameters to capture the input dynamics into its latent space and *under-fits*, while for $M_Q > 8$, the posterior network starts over-fitting, reducing the success rate again.

Regarding the *state-transition* network, Fig. 4 shows that the higher the number of neurons M_P , the flatter the success rate curves become, leading to higher performance. The state transition network does not seem to over-fit as M_P is increased (for $\lambda_P = 10^{-4}$ kept fixed). Rather, Fig. 4 indicates that a higher state-transition network capacity is beneficial for capturing important dynamics in the latent space, at the output of the posterior network.

4.3 Impact of the Sparsity of the Output Activity in the Posterior and State Transition Networks

Fig. 5 and 6 show the effect of sweeping the *sparsity-defining* hyper-parameters λ_Q and λ_P in both the *posterior* and *state-transition* networks. For the posterior network, Fig. 5 shows that the success rate performance initially grows as λ_Q is increased from $\lambda_Q = 10^{-6}$ to $\lambda_Q = 10^{-5}$. Doing so, the non-linearity of the posterior network is increased, better capturing observation features into its

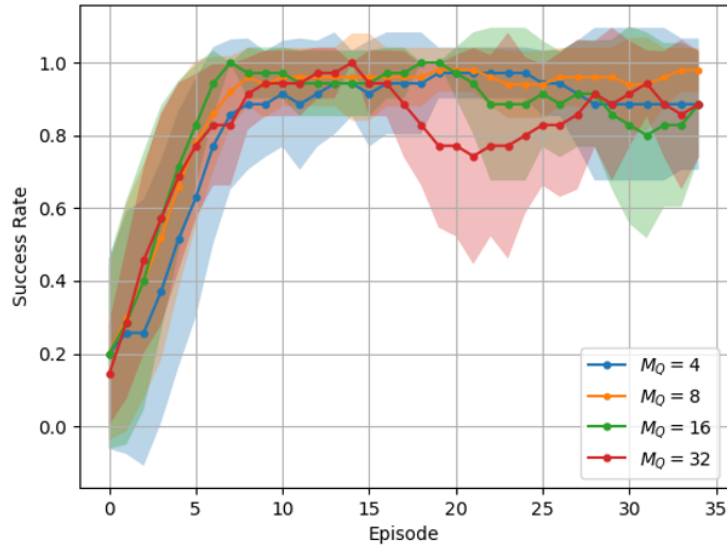


Fig. 3. Impact on the success rate when changing the *number of neurons* M_Q in the *posterior network*.

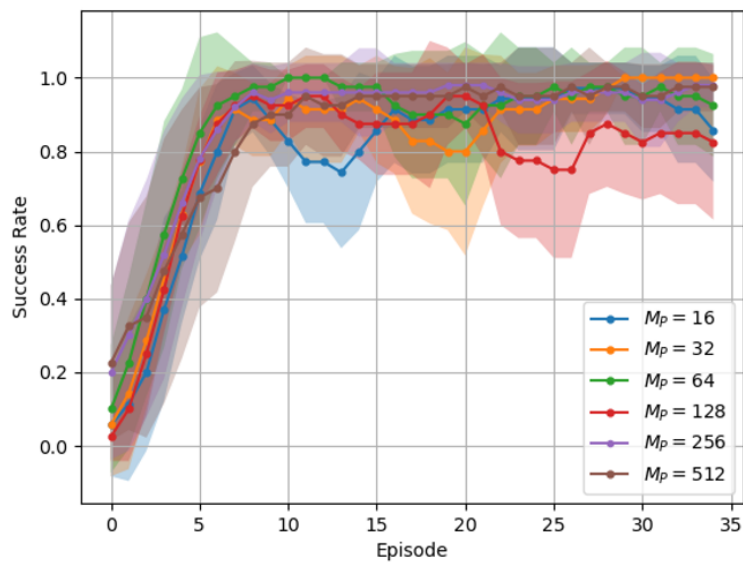


Fig. 4. Impact on the success rate when changing the *number of neurons* M_P in the *state transition network*.

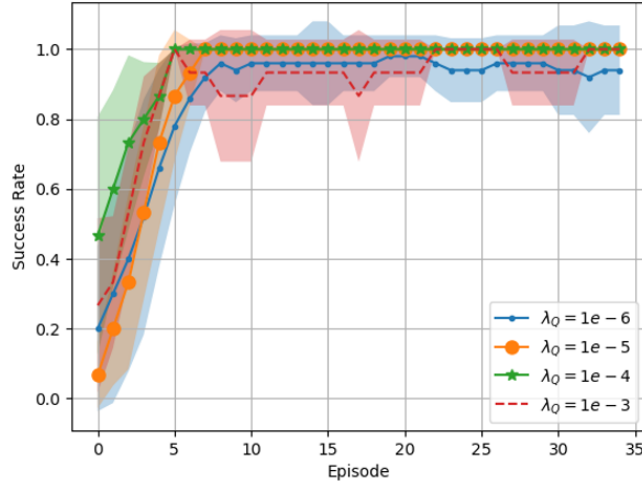


Fig. 5. Impact on the success rate when changing the *sparsity hyper-parameter* λ_Q in the *posterior network*.

latent space. Then, as λ_Q grows past $\lambda_Q = 10^{-4}$, the success rate degrades again, indicating a too strong posterior network non-linearity.

Regarding the *state-transition* network, Fig. 6 shows that the lower λ_P , the higher the success rate becomes. This suggests that making the state-transition network *more linear* (i.e., lower λ_P) better captures the dynamics of the latent space produced by the posterior network (other parameters kept fixed).

4.4 Impact of the Time-Lag Buffer Length on Task Performance

Fig. 7 shows how the length L_{buf} of the time-lag buffer impacts the achieved success rate. Initially, as L_{buf} increases, the success rate increases as well, due to an increased availability of past latent states used by the state-transition network to estimate the next expected state. Then, as L_{buf} is further increased for $L_{buf} > 20$, the success rate drops again due to the addition of latent states *from deep in the past* that are less useful for estimating the present dynamics.

4.5 Comparing Hebbian AIF against the Use of a Replay Buffer and against Q-learning

Fig. 8 compares the success rate obtained using our proposed Hebbian AIF system against *a)* the use of a replay buffer during learning and *b)* the use of a Q-learning agent. Experience replay is done by saving the history of observation-action pairs in a buffer after each episode. After the end of the episode, a past experience is randomly selected and used to train the Hebbian AIF system for one episode.

Regarding the Q-learning setup, we use a standard Q-table learning approach [22], with the python implementation proposed in [33].

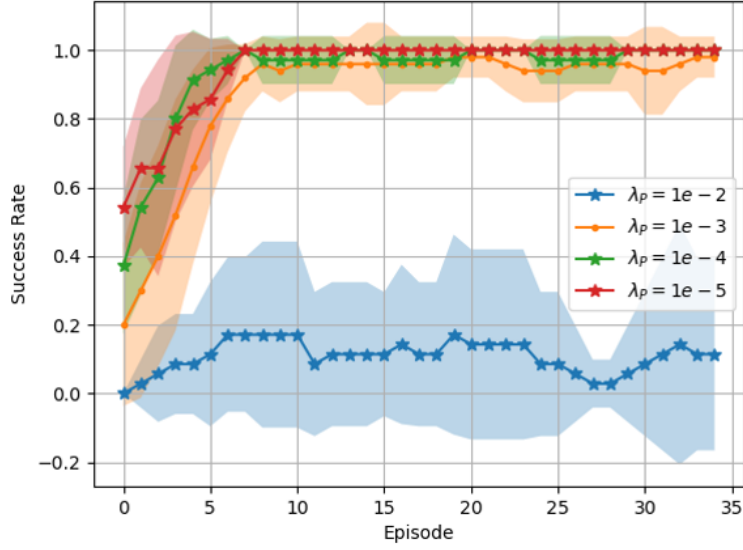


Fig. 6. Impact on the success rate when changing the *sparsity* λ_P in the *state transition network*.

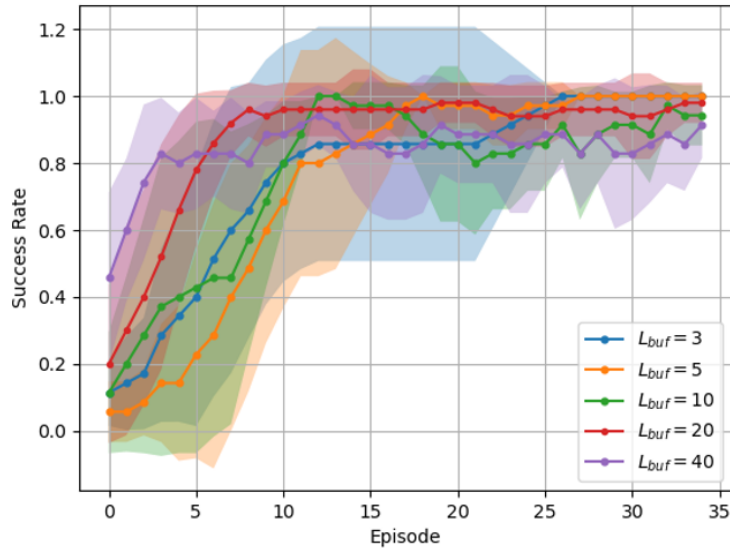


Fig. 7. Success rate when changing the *time-lag buffer length* L_{buf} .

Fig. 8 shows that our Hebbian AIF system converges much faster than the Q-learning system and behaves in a comparable manner to the Hebbian AIF setup with a *replay buffer*. Indeed, the Q-learning agent needs much more episodes in order to converge, despite the fact that it utilizes the *dense rewards* provided by the Mountain Car environment [21] (versus *unsupervised* learning in the case of Hebbian AIF). This confirms prior observations about the efficient convergence of AIF systems, due to their ability to learn a generative model of environment dynamics (versus supervised learning of a Q-table) [17].

Finally, it is interesting to note that, compared to the Deep AIF results reported in [17] (using a fully-connected 2-hidden-layer network trained through backprop), the Hebbian AIF system proposed in this work eventually reaches $\sim 100\%$ success rate (see red curve in Fig. 6) while the system in [17] reaches $\sim 95\%$, motivating further investigations of Hebbian learning for AIF systems.

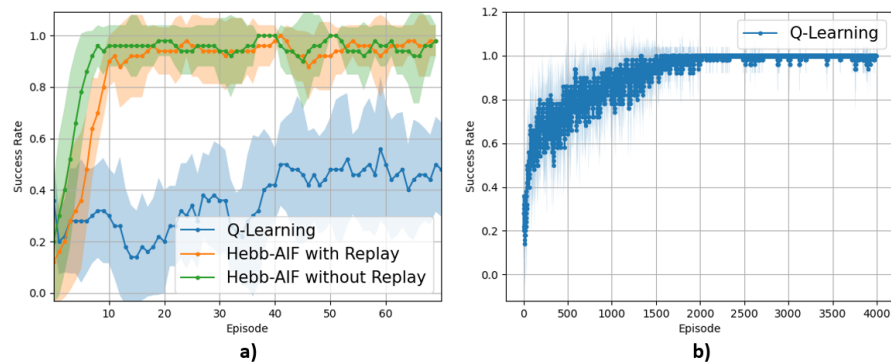


Fig. 8. Hebbian AIF versus the use of a *replay buffer* and *Q-learning* (a). Q-learning needs two orders of magnitude more episodes in order to converge (b).

5 Conclusion

This paper has investigated how neural ensembles equipped with local Hebbian plasticity can perform active inference for the control of dynamical agents. First, a Hebbian network architecture performing joint dictionary learning and sparse coding has been introduced for implementing both the posterior and the state-transition models forming our generative Active Inference system. Then, it has been shown how Free Energy minimization can be performed by the proposed Hebbian AIF system. Finally, extensive experiments for parameter exploration and benchmarking have been performed to study the impact of the network parameters on the task performance. Experimental results on the Mountain Car environment show that the proposed system outperforms the use of Q-learning, while *not requiring* the use of a replay buffer during learning, motivating *future investigations* of using Hebbian learning for designing active inference systems.

Acknowledgement

This research was partially funded by a Long Stay Abroad grant from the Flemish Fund of Research - Fonds Wetenschappelijk Onderzoek (FWO) - grant V413023N. This research received funding from the Flemish Government under the “Onderzoeksprogramma Artificiële Intelligentie (AI) Vlaanderen” programme.

References

1. Bruno A. Olshausen, David J. Field (1997). "Sparse coding with an overcomplete basis set: A strategy employed by V1?." *Vision Research*, 37(23), 3311-3325.
2. Fang, M.S., Mudigonda, M., Zarccone, R., Khosrowshahi, A., Olshausen, B. (2022). "Learning and Inference in Sparse Coding Models With Langevin Dynamics." *Neural Computation*, 34(8), 1676-1700.
3. Lee, H., Battle, A., Raina, R., Ng, A. (2006). "Efficient sparse coding algorithms." In *Advances in Neural Information Processing Systems*. MIT Press.
4. Ali Safa, Ilja Ocket, André Bourdoux, Hichem Sahli, Francky Catthoor, Georges Gielen. (2022). "A New Look at Spike-Timing-Dependent Plasticity Networks for Spatio-Temporal Feature Learning."
5. Friston, K., Kiebel, S. (2009). "Predictive coding under the free-energy principle." *Philosophical transactions of the Royal Society of London. Series B, Biological sciences*, 364, 1211-21.
6. Friston, K. Does predictive coding have a future?. *Nat Neurosci* 21, 1019–1021 (2018). <https://doi.org/10.1038/s41593-018-0200-7>
7. Umair Zahid, Qinghai Guo, Zafeirios Fountas.(2023). "Predictive Coding as a Neuromorphic Alternative to Backpropagation: A Critical Evaluation."
8. Olshausen, B., Field, D. (1996). "Emergence of simple-cell receptive field properties by learning a sparse code for natural images." *Nature*, 381, 607-609.
9. Safa, A., Ocket, I., Bourdoux, A., Sahli, H., Catthoor, F., Gielen, G. (2022). "Event Camera Data Classification Using Spiking Networks with Spike-Timing-Dependent Plasticity." In *2022 International Joint Conference on Neural Networks (IJCNN)* (pp. 1-8).
10. Guo-qiang Bi, Mu-ming Poo (1998). "Synaptic Modifications in Cultured Hippocampal Neurons: Dependence on Spike Timing, Synaptic Strength, and Postsynaptic Cell Type." *Journal of Neuroscience*, 18(24), 10464–10472.
11. Rao, R., Ballard, D. (1999). "Predictive coding in the visual cortex: a functional interpretation of some extra-classical receptive-field effects." *Nature neuroscience*, 2(1), 79–87.
12. A. Safa, I. Ocket, A. Bourdoux, H. Sahli, F. Catthoor and G. G. E. Gielen, "STDP-driven Development of Attention-based People Detection in Spiking Neural Networks," in *IEEE Transactions on Cognitive and Developmental Systems*, 2022, doi: 10.1109/TCDS.2022.3210278.
13. Neftci, E., Das, S., Pedroni, B., Kreutz-Delgado, K., Cauwenberghs, G. (2014). "Event-driven contrastive divergence for spiking neuromorphic systems." *Frontiers in Neuroscience*, 7.
14. Dmitry Krotov, John J. Hopfield (2019). "Unsupervised learning by competing hidden units." *Proceedings of the National Academy of Sciences*, 116(16), 7723-7731.
15. Parr, T., Pezzulo, G., Friston, K. (2022). "Active Inference: The Free Energy Principle in Mind, Brain, and Behavior." *The MIT Press*.
16. Isomura, T., Shimazaki, H. Friston, K.J. "Canonical neural networks perform active inference." *Commun Biol* 5, 55 (2022). <https://doi.org/10.1038/s42003-021-02994-2>
17. Çatal, O., Wauthier, S., De Boom, C., Verbelen, T., Dhoedt, B. (2020). "Learning Generative State Space Models for Active Inference." *Frontiers in Computational Neuroscience*, 14.
18. Ueltzhöffer, K. "Deep active inference." *Biol Cybern* 112, 547–573 (2018). <https://doi.org/10.1007/s00422-018-0785-7>

19. Fountas, Z., Sajid, N., Mediano, P., Friston, K. (2020). "Deep active inference agents using Monte-Carlo methods." In *Advances in Neural Information Processing Systems* (pp. 11662–11675). Curran Associates, Inc..
20. Van de Maele, T., Verbelen, T., Çatal, O., De Boom, C., Dhoedt, B. (2021). "Active Vision for Robot Manipulators Using the Free Energy Principle." *Frontiers in Neurobotics*, 15.
21. Brockman, G., Cheung, V., Pettersson, L., Schneider, J., Schulman, J., Tang, J., Zaremba, W. (2016). "Openai gym." arXiv preprint arXiv:1606.01540.
22. Sutton, R., Barto, A. (2018). "Reinforcement Learning: An Introduction." The MIT Press.
23. Ororbia, A. G., Mali, A. (2022). "Backprop-Free Reinforcement Learning with Active Neural Generative Coding." *Proceedings of the AAAI Conference on Artificial Intelligence*, 36(1), 29-37.
24. Alexander Ororbia, Ankur Mali. "Active Predicting Coding: Brain-Inspired Reinforcement Learning for Sparse Reward Robotic Control Problems." *IEEE International Conference on Robotics and Automation (ICRA) 2023*.
25. Yuchen Liang, Chaitanya Ryali, Benjamin Hoover, Leopold Grinberg, Saket Navlakha, Mohammed J Zaki, Dmitry Krotov (2021). "Can a Fruit Fly Learn Word Embeddings?." In *International Conference on Learning Representations*.
26. Ablin, P., Moreau, T., Massias, M., Gramfort, A. (2019). "Learning step sizes for unfolded sparse coding." In *Advances in Neural Information Processing Systems*. Curran Associates, Inc.
27. Tsung-Han Lin, Ping Tak Peter Tang (2019). "Sparse Dictionary Learning by Dynamical Neural Networks." In *International Conference on Learning Representations*.
28. Friston, K. "The free-energy principle: a unified brain theory?." *Nat Rev Neurosci* 11, 127–138 (2010). <https://doi.org/10.1038/nrn2787>
29. J. R. Hershey and P. A. Olsen, "Approximating the Kullback Leibler Divergence Between Gaussian Mixture Models," 2007 IEEE International Conference on Acoustics, Speech and Signal Processing - ICASSP '07, Honolulu, HI, USA, 2007, pp. IV-317-IV-320, doi: 10.1109/ICASSP.2007.366913.
30. Kim, E., Lawson, E., Sullivan, K., Kenyon, G. (2019). "Spatiotemporal Sequence Memory for Prediction Using Deep Sparse Coding." In *Proceedings of the 7th Annual Neuro-Inspired Computational Elements Workshop*. Association for Computing Machinery.
31. P. J. Werbos, "Backpropagation through time: what it does and how to do it," in *Proceedings of the IEEE*, vol. 78, no. 10, pp. 1550-1560, Oct. 1990, doi: 10.1109/5.58337.
32. Schwartenbeck, P., FitzGerald, T., Dolan, R., Friston, K. (2013). "Exploration, novelty, surprise, and free energy minimization." *Frontiers in Psychology*, 4.
33. <https://gist.github.com/gkhayes/3d154e0505e31d6367be22ed3da2e955> (accessed May 1 2023)